Analysis of the Breakdown Characterization Method in GaN-Based HEMTs

Sheng Lei Zhao, Bin Hou, Wei Wei Chen, Min Han Mi, Jia Xin Zheng, Jin Cheng Zhang, Xiao Hua Ma, *Member, IEEE*, and Yue Hao, *Senior Member, IEEE*

***Abstract*—In this paper, we carried out an analysis of the breakdown characterization method by the investigation on off-state leakage currents and breakdown curves. For conventional breakdown, seven kinds of breakdown curves are summarized and it is found that only two of them can be shown by the conventional three-terminal breakdown characterization method reasonably. For the other five kinds of breakdown curves, the value of the gate leakage current is larger than that of the drain leakage current for a certain drain-bias range. Besides, the source leakage current cannot represent the buffer leakage current, and the values and signs of them are different. These problems contradict the conventional characterization method, indicating that the conventional method should be modified to characterize the breakdown mechanisms correctly. The similar problems also exist for time-dependent breakdown. The buffer and drain-gate leakage currents were obtained by a simple method and the conventional breakdown characterization method was modified by using these two currents. The problems in the conventional breakdown characterization method are solved by using the modified method. Experiments indicate that the modified breakdown characterization method is crucial to investigate the breakdown mechanisms, especially when source-gate leakage current cannot be neglected compared with the buffer leakage current.**

***Index Terms*—Breakdown characterization method, breakdown curves, breakdown mechanisms, GaN-based high-electron-mobility transistors (HEMTs), off-state leakage currents.**

I. Introduction

In recent years, GaN-based high-electron-mobility transistors (HEMTs) are considered to be excellent candidates for power electronics applications due to the superior characteristics, such as high breakdown voltage ($V_{\rm BR}$), low specific on-resistance, and small gate charge [1]–[4]. Silicon MOSFETs have reached their limits in terms of power density and switching frequency nowadays, whereas GaN-based HEMTs possess the ability to exceed these limits of silicon MOSFETs. A 3-kW 400 V:800 V hard-switched boost converter based on GaN-based HEMTs has been fabricated with 99% efficiency at 100 kHz [5]. A synchronous buck converter based on GaN-based HEMTs could provide more than 10-W output power with efficiencies greater than 95% when operated at 10 MHz [6]. GaN-based HEMTs are the most important components in these GaN-based applications, and numerous studies have been carried out on these devices. There is no doubt that breakdown voltage is a very important figure of merit for GaN-based HEMTs. The device breakdown can be induced by avalanche breakdown, gate leakage, buffer leakage and so on. In order to investigate the breakdown mechanisms, the conventional 3-D breakdown characterization method has been used widely [7]–[15].

Although the conventional 3-D breakdown characterization method is generally used to analyze the breakdown mechanisms, very serious problems emerge during this procedure, which still has not been paid attention to. In the conventional method, three off-state leakage currents, I_D, I_S and I_G, are measured to analyze the breakdown mechanisms. Here I_D is the drain leakage current, I_S is the source leakage current, and I_G is the gate leakage current. In general, the drain leakage current is the sum of source leakage current and the gate leakage and the value of the drain leakage current should be higher than any one of the other two. However, the gate leakage current was shown to be higher than the drain leakage current during the breakdown characterization in [12, Fig. 9]. The buffer leakage current is the bulk punch through leakage current under the depletion region of the transistor gate, and it should increase with the increase of the drain bias. In previous studies, the source leakage current was usually considered as the buffer leakage current. The source leakage current firstly decreased, and then increased with the increase of the drain bias in [13, Fig. 9(b)], which contradicts the trend of the buffer leakage current. Actually, these two strange phenomena not only exist in these two laboratories, but also exist in many other laboratories [14], [15], including our laboratory. Therefore, some problems must exist in the conventional breakdown characterization method and these problems are needed to be explained and solved by scientific research.

Among our many kinds of devices, we choose two kinds of GaN-based HEMTs, a kind of conventional HEMTs and a kind of HEMTs with AlGaN back barrier layer, to investigate these problems. These problems have been observed in the devices and the reduction of the buffer leakage current by using the back barrier layer cannot be observed by monitoring the source leakage current, indicating that the conventional breakdown characterization method is not suitable to characterize the breakdown mechanisms of these devices. In this paper, all the

Manuscript received November 25, 2014; revised February 9, 2015; accepted March 10, 2015. Date of publication March 25, 2015; date of current version September 29, 2015. This work was supported by the National Natural Science Foundation of China under Grants 61334002, 61306017, and 61204085. Recommended for publication by Associate Editor A. Lindemann.

S. L. Zhao, M. H. Mi, J. C. Zhang, and Y. Hao are with the Key Laboratory of Wide Band Gap Semiconductor Materials and Devices, School of Microelectronics, Xidian University, Xi'an 710071, China (e-mail: shleilong@126.com; miminhan@qq.com; jchzhang@xidian.edu.cn; yhao@xidian.edu.cn).

B. Hou, W. W. Chen, J. X. Zheng, and X. H. Ma are with the School of Advanced Materials and Nanotechnology, Xidian University, Xi'an 710071, China (e-mail: hobbyzhuquanlinxi@163.com; cwwaw@126.com; zheng2510285@163.com; xhma@xidian.edu.cn).

Color versions of one or more of the figures in this paper are available online at http://ieeexplore.ieee.org.

Digital Object Identifier 10.1109/TPEL.2015.2416773

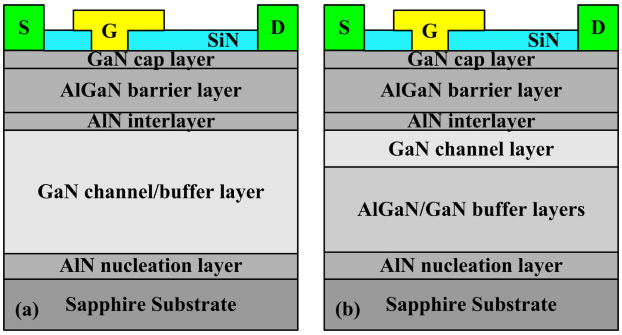

Fig. 1. Schematic cross sections of (a) conventional AlGaN/GaN HEMTs and (b) AlGaN/GaN DH HEMTs.

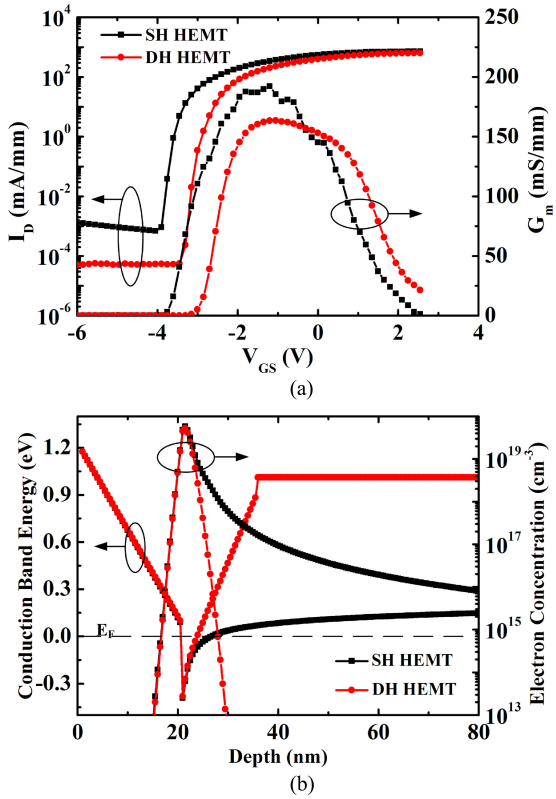

Fig. 2. (a) Transfer characteristics of the conventional AlGaN/GaN HEMT and DH HEMT. The conventional AlGaN/GaN HEMT is referred to as the single-heterojuntion (SH) HEMT. (b) Calculated conduction band diagrams and electron distributions of the SH HEMT and DH HEMT.

off-state leakage currents and the kinds of breakdown curves have been analyzed carefully. It is found that the source-gate leakage current is the main reason for these problems. Because of the source-gate leakage current, the value of the gate leakage current may be larger than that of the drain leakage current for a certain drain-bias range, and the source leakage current cannot represent the buffer leakage current if the source-gate leakage current is not negligible. On the contrary, the source-gate leakage current is neglected in the conventional breakdown characterization method.

The main study of this paper includes three parts. In Section II, two kinds of GaN-based HEMTs were measured and the problems of the conventional breakdown characterization method were presented. In Section III, eight leakage currents were studied and seven kinds of breakdown curves were summarized for conventional breakdown. The problems discussed above exist in five kinds of breakdown curves, which have been explained detailedly. The similar problems also exist for time-dependent breakdown. In order to illustrate the relation between breakdown curves and breakdown mechanisms, each leakage current component is discussed, and the relation between leakage currents and breakdown mechanisms has been analyzed carefully. In Section IV, a simple method to extract the buffer leakage current was proposed. Based on this extraction method, the conventional breakdown characterization method was modified and the modified method was proved to be effective to solve the discussed problems by the experiments.

II. Device Structures and Characteristics

As shown in Fig. 1, two kinds of GaN-based HEMTs, namely conventional AlGaN/GaN HEMTs and AlGaN/GaN/AlGaN double-heterojunction (DH) HEMTs, were fabricated to investigate the breakdown characterization method. The two heterojunction structures were grown on sapphire substrates by metal-organic chemical vapor deposition. For the conventional HEMT, a 1.5-μm GaN channel/buffer layer was grown. For the DH HEMT, the buffer layer contains a 0.75-μm GaN layer and a 0.75-μm linearly graded $\mathrm{Al}_x\mathrm{Ga}_{1-x}\mathrm{N}$ layer with Al maximum content of 7% at the interface to a 15-nm GaN channel layer. The aim of the grading is to reduce the polarization-induced doping and avoid the generation of a secondary channel. The two samples have a 1-nm AlN spacer layer followed by a 21-nm $\mathrm{Al}_{0.3}\mathrm{Ga}_{0.7}\mathrm{N}$ barrier layer and a 1.5-nm GaN cap layer. The sheet carrier concentrations are 9.0×10^{12} and 8.0×10^{12} cm^{-2} for the conventional HEMT and DH HEMT, respectively. The device fabrication commenced with mesa isolation by reactive ion etching using Cl_2 plasma. Ohmic metal was formed using Ti/Al/Ni/Au while Schottky gate using Ni/Au/Ni layers. The tested devices for the two kinds of GaN-based HEMTs have a gate length $L_G = 1$ μm, a gate-source spacing $L_{\mathrm{GS}} = 1$ μm, and a gate-drain spacing $L_{\mathrm{GD}} = 3$ μm.

Fig. 2(a) shows the transfer characteristics of the SH HEMT and the DH HEMT. The maximum drain current at $V_{\mathrm{GS}} = 2.5$ V reaches 713 mA/mm for the SH HEMT and 631 mA/mm for the DH HEMT, respectively. As shown in Fig. 2(b), the conduction band diagrams and electron distributions of DH and SH HEMTs are calculated by self-consistently solving a 1-D Poisson–Schrödinger equation. The 2-D electron gas (2DEG) confinement would be enhanced by using the AlGaN back barrier layer, and the buffer leakage current can be reduced in the DH HEMT compared with the SH HEMT [16], [17]. The off-state drain leakage current was reduced from 1.32×10^{-3} to 5.04×10^{-5} mA/mm at $V_{\mathrm{GS}} = -6$ V, leading to the increase of $I_{\mathrm{on}}/I_{\mathrm{off}}$ from 5.4×10^5 to 1.3×10^7.

The conventional three-terminal breakdown characteristics of the AlGaN/GaN SH and DH HEMTs are shown in Fig. 3. The breakdown voltage is defined as the drain voltage with the drain leakage current reaching 1 mA/mm. The breakdown voltage is

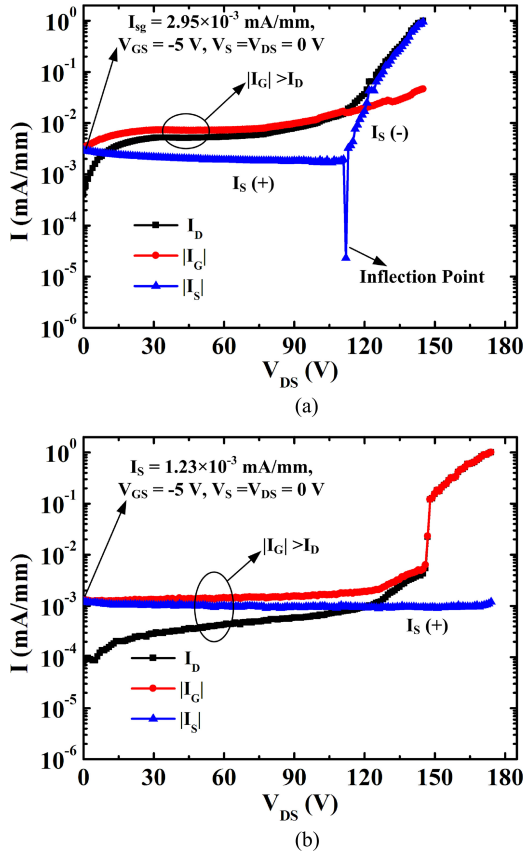

Fig. 3. Conventional three-terminal breakdown characteristics of the AlGaN/GaN (a) SH HEMT and (b) DH HEMT with VGS = –5 V. The sign of the current flowing into the electrode is defined as positive (+). Otherwise, it was defined as negative (−).

improved from 145 V for the SH HEMT to 174 V for the DH HEMT. The improvement of the breakdown voltage results from the reduced buffer leakage by using the AlGaN buffer layer. By using the conventional breakdown characterization method, we can obtain the information that the SH HEMT breakdown is induced by the buffer leakage and the DH HEMT breakdown is induced by the gate leakage. However, three problems emerge in Fig. 3.

1) In general, the drain leakage current I_D is the sum of source leakage current I_S and the gate leakage I_G and the value of the drain leakage current should be higher than any one of the other two. Paradoxically, I_G in the two HEMTs are higher than I_D for $V_{\rm DS} < 100$ V.
2) The source leakage current was usually considered as the buffer leakage current. The buffer leakage should be reduced by using AlGaN back barrier layer. In contrast, I_S of the DH HEMT does not decrease evidently compared with that of the SH HEMT.
3) The buffer leakage current is the bulk punch through leakage current under the depletion region of the transistor gate. The buffer leakage flows from drain to source, and I_S should be negative if it can represent the buffer leakage. In addition, the buffer leakage current should increase with the increase of the drain bias.

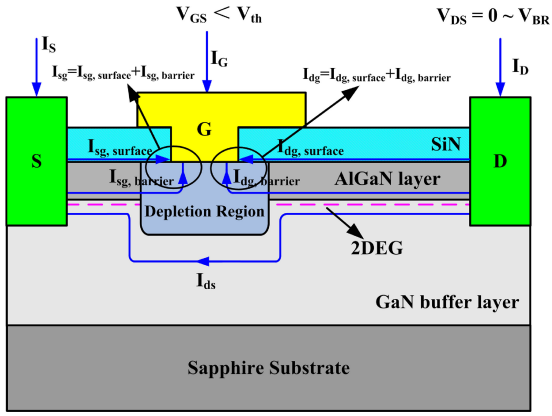

Fig. 4. Off-state leakage currents in GaN-based HEMTs during the breakdown measurements.

In Fig. 3(a), I_S of the SH HEMT is positive and decreases with the increase of the drain bias for $V_{\rm DS} < 112$ V. The sign and value variation trend of I_S are opposite to those of the buffer leakage. There exists a minimum I_S value at $V_{\rm DS} = 112$ V for the SH HEMT. I_S becomes negative and increases with the increase of $V_{\rm DS}$ for $V_{\rm DS} > 112$ V. For the DH HEMT, I_S is positive and decreases all through the breakdown measurements. Therefore, it should be discussed that whether the source leakage current can represent the buffer leakage current.

In order to solve these problems, all the off-state leakage currents and the kinds of breakdown curves should be analyzed carefully, which will be carried out in Section III.

III. Discussions of Leakage Currents and Breakdown Curves

A. Leakage Currents and Breakdown Curves

With $V_{\rm GS} < V_{\rm th}$, I_S, I_G, and I_D are all off-state leakage currents. As shown in Fig. 4, I_S, I_G, and I_D can be monitored during the breakdown measurements, while other five leakage currents, $I_{\rm sg,surface}$, $I_{\rm dg,surface}$, $I_{\rm sg,barrier}$, $I_{\rm dg,barrier}$, and $I_{\rm ds}$, are the off-state leakage currents inside the devices, and they cannot be obtained directly. $I_{\rm sg,surface}$ and $I_{\rm dg,surface}$ are the leakage currents along the AlGaN surface. $I_{\rm sg,barrier}$ and $I_{\rm dg,barrier}$ are the barrier leakage currents through the AlGaN barrier. The source-gate leakage current $I_{\rm sg}$ consists of $I_{\rm sg,surface}$ and $I_{\rm sg,barrier}$, while the drain-gate leakage current $I_{\rm dg}$ consists of $I_{\rm dg,surface}$ and $I_{\rm dg,barrier}$. $I_{\rm sg}$ and $I_{\rm dg}$ form the gate leakage current I_G. The buffer leakage current, $I_{\rm ds}$, flows from drain terminal to source terminal through the buffer layer underneath the depletion region of the gate terminal.

As shown in Fig. 4, the source leakage current is not the buffer leakage current. I_S is the vector sum of $I_{\rm ds}$ and $I_{\rm sg}$, which flow in different direction. The sign of I_S would be opposite to $I_{\rm ds}$ if the absolute value of $I_{\rm sg}$ is larger than that of $I_{\rm ds}$. The gate bias $V_{\rm GS}$ is set as a constant value during the breakdown measurements, so $I_{\rm sg}$ would be kept as a constant value. In contrast, $I_{\rm ds}$ increases with the increase of the drain bias $V_{\rm DS}$. In the SH HEMT as shown in Section II, the absolute value of $I_{\rm sg}$ is larger than that of $I_{\rm ds}$ for $V_{\rm DS} < 112$ V. As a result, the sign of I_S is positive,

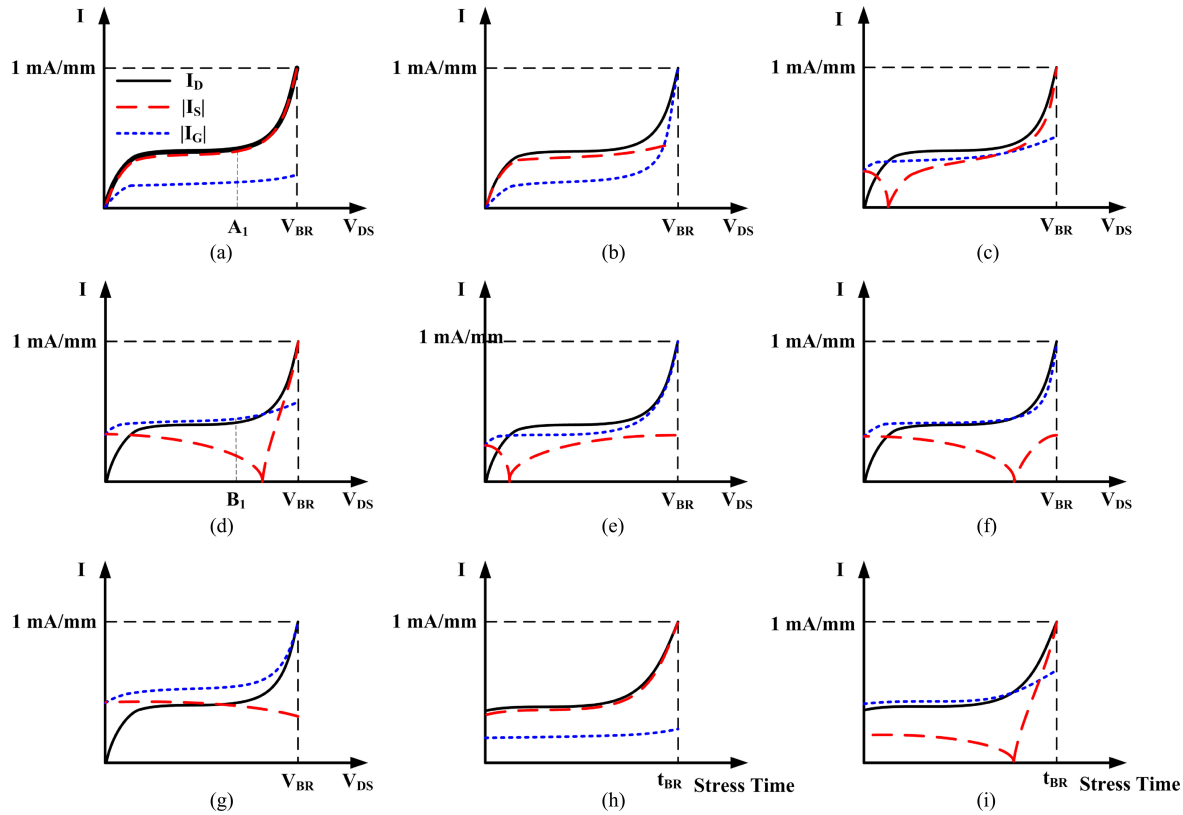

Fig. 5. Nine kinds of breakdown curves for (a)–(g) conventional breakdown and (h), (i) time-dependent breakdown, named types A-I. The leakage currents on the y-axis for types A-I and stress time on the x-axis for types H and I are in a log scale.

opposite to that of $I_{\rm ds}$, and the value of I_S would decrease with the increase of $I_{\rm ds}$. With the increase of $I_{\rm ds}$, $|I_{\rm ds}|$ exceeds $|I_{\rm sg}|$ for $V_{\rm DS} > 112$ V. The sign of I_S is changed to negative, the same as that of $I_{\rm ds}$, and I_S would increase with the increase of $I_{\rm ds}$. For the DH HEMT, $|I_{\rm ds}|$ is smaller than $|I_{\rm sg}|$ all through the breakdown measurements. As a result, the sign of I_S is opposite to that of $I_{\rm ds}$, and I_S decreases with the increase of $I_{\rm ds}$ during the whole breakdown measurements. Since the source leakage current is not the buffer leakage current, the reduction of the buffer leakage current possibly cannot be observed by monitoring the source leakage current in the two kinds of GaN-based HEMTs. I_D is the vector sum of I_G and I_S, not the sum of $|I_G|$ and $|I_S|$. I_D is positive and I_G is negative. $|I_G|$ would be higher than I_D if I_S is positive. Changing to another way of analysis, I_D consists of the two leakage currents $I_{\rm dg}$ and $I_{\rm ds}$, and I_G consists of the two leakage currents $I_{\rm dg}$ and $I_{\rm sg}$. $|I_G|$ would be higher than I_D if $|I_{\rm sg}|$ is larger than $|I_{\rm ds}|$.

Based on the analysis of leakage currents, we have summarized seven possible kinds of conventional breakdown curves as shown in Fig. 5(a)–(g). Device breakdown types include buffer-induced breakdown (A, C, and D) and gate-induced breakdown (B, E, F, and G) types. For types A and B, $|I_{\rm sg}|$ is smaller than $|I_{\rm ds}|$ at the initial bias. When $V_{\rm DS}$ increases to a certain value, $|I_{\rm ds}|$ would be much higher than $|I_{\rm sg}|$. As a result, the source-gate leakage $I_{\rm sg}$ can be neglected in these two situations. Therefore, the value and the sign of source leakage current I_S are almost the same as those of the buffer leakage current $I_{\rm ds}$ for types A and B.

If $|I_{\rm sg}|$ is larger than $|I_{\rm ds}|$ at the initial bias, breakdown curves would belong to types C–G. For the initial point of the breakdown types C–G curves (e.g., $V_{\rm GS} = -5$ V, $V_S = V_{\rm DS} = 0$ V), $I_{\rm ds}$ is zero, the absolute value of I_S equals $I_{\rm sg}$, and the difference between I_G and I_S is $I_{\rm dg}$. For GaN-based HEMTs, the gate-drain spacing is always larger than the gate-source spacing, and the value of $I_{\rm dg}$ is much smaller than $I_{\rm sg}$ at the initial bias. Hence, the value of $I_{\rm dg}$ is very small compared with that of I_G and I_S. As a result, I_G and I_S appear to overlap at the initial point. Besides, the increase of I_G results from the increase of $I_{\rm dg}$.

For types C and E, $|I_{\rm ds}|$ exceeds $|I_{\rm gs}|$ at a low drain bias. For types D and F, $|I_{\rm ds}|$ exceeds $|I_{\rm gs}|$ at a high drain bias. The point at which $|I_{\rm ds}|$ begins to exceed $|I_{\rm gs}|$ is the inflection point of the reduction and increase of $|I_S|$. Before this inflection point, the sign of I_S is positive, opposite to that of $I_{\rm ds}$. After this point, the sign of I_S is negative, the same as that of $I_{\rm ds}$. In contrast, if $|I_{\rm ds}|$ cannot exceed $|I_{\rm gs}|$ for the whole measurements, the breakdown type would become to type G. There is no inflection point of I_S in type G, and the sign of I_S is opposite to that of $I_{\rm ds}$ all through the breakdown measurements.

In order to understand the relation between the seven kinds of breakdown curves, we assume that the $I_{\rm ds}$ in these types have the same values. When $|I_{\rm sg}|$ is smaller than $|I_{\rm ds}|$ at the initial point, breakdown curves would be types A and B as shown in Fig. 6. Type A is buffer-induced breakdown and type B is gate-induced breakdown. When $|I_{\rm sg}|$ increases to a value higher than $|I_{\rm ds}|$, types A and B would become to types C and

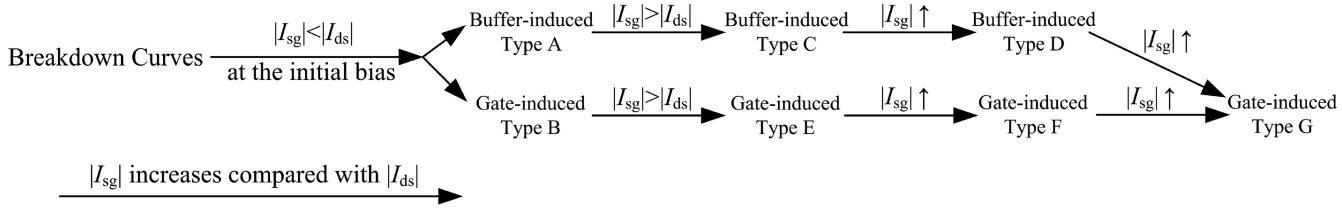

Fig. 6. Schematic of the relation between breakdown types A $\sim$ G.

E respectively, and the inflection point begins to emerge. If $|I_{\rm sg}|$ continue to increase, types C and E will be changed to D and F respectively and the inflection would move positively along the drain-bias axis. When $|I_{\rm sg}|$ increases to a value much higher than $|I_{\rm ds}|$, both buffer-induced breakdown type D and gate-induced breakdown type F would become gate-induced breakdown type G, and the inflection point is out of the breakdown measurements range. The practical breakdown curves may not be so smooth as the breakdown curves drawn in Fig. 5. Besides, some of the practical breakdown curves may not seem like these seven kinds of breakdown curves. However, those strange breakdown curves can be explained by these seven kinds of breakdown curves. The I_G of types C–G is large, which does not mean that I_G is really large, but means that the value of I_G is large compared with that of $I_{\rm ds}$. Thus, the devices corresponding to these breakdown types can be used in applications as types A and B.

The conventional three-terminal breakdown characterization method can apply to types A and B. Because of the source-gate leakage $I_{\rm gs}$, I_S deviates from $I_{\rm ds}$ severely and $|I_G|$ of types C–G are higher than I_D for a certain drain-bias range. I_S and I_G are not suitable to characterize the breakdown mechanisms for types C–G. Actually, $I_{\rm ds}$ and $I_{\rm dg}$ are the leakage currents which form I_D and raise I_D to the breakdown criterion. The conventional method should be modified for types C–G by using $I_{\rm ds}$ and $I_{\rm dg}$ instead of I_S and I_G.

B. Relation Between Leakage Currents and Breakdown Mechanisms

Breakdown curves are comprised of leakage currents. In order to illustrate the relation between breakdown curves and breakdown mechanisms, the relation between leakage currents and breakdown mechanisms should be analyzed carefully. At first, each leakage current component will be discussed.

When gate is reversely biased, the gate leakage current is comprised of surface leakage and barrier leakage. Fig. 7(a) shows the mechanisms of surface leakage current. The electrons that tunnel from the gate electrode can accumulate on the AlGaN surface next to the gate, and then conduct along the surface states by a trap-to-trap hopping mechanism or Poole–Frenkel (PF) emission, creating the gate-to-drain surface leakage current [18]–[20]. Thermionic emission (TE) and tunneling emission are likely involved in the hopping conduction, and the hopping conduction can be enhanced by high temperature and high electric field [18]. The PF emission is also a trap-assisted emission, and the extracted energy barrier height of electrons emitting from trapped state near Fermi energy level into a threading dislocations-related continuum state $E_{\rm dis}$ is 0.38 eV [19]. PF

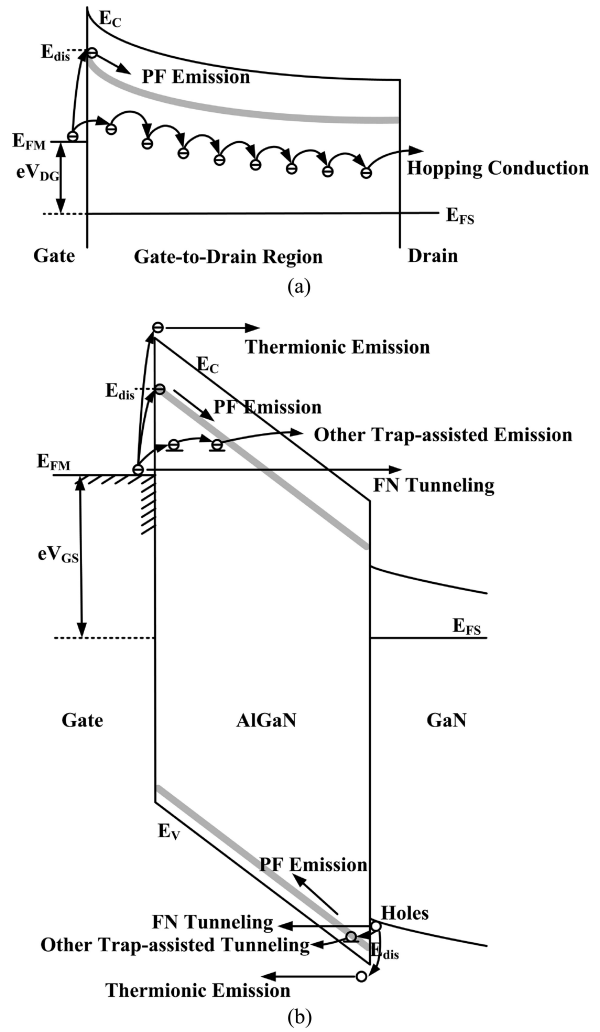

Fig. 7. Energy band diagrams of AlGaN/GaN HEMTs illustrating (a) surface leakage current mechanisms and (b) barrier leakage current mechanisms with gate reversely biased.

emission current can be given by [21]

$$J_{PF} = CE \exp\left[-\frac{q(\phi_t - \sqrt{(qE/\pi\varepsilon_i)})}{kT}\right] \quad (1)$$

where C is a constant, E denotes the electric field in the AlGaN barrier at the metal–semiconductor interface, ϕ_t is the barrier height of the electron emission from the trapped state, ε_i is the permittivity of the semiconductor at high frequency. The value of PF emission current is dependent on temperature and electric field.

At a low electric field, the hopping conduction is the main mechanism of the surface leakage. At a high electric field, the PF emission would govern the main surface electrons transportation [19]. The surface leakage induced breakdown exhibited a negative temperature coefficient, indicating the breakdown mechanism is thermal runaway rather than impact ionization [20]. The surface leakage current can be obtained by double gates structure [22], and can be reduced effectively by surface treatment and high-quality SiN passivation [19].

The electrons at the gate side can travel through the AlGaN barrier layer to the 2DEG channel, resulting in the barrier leakage. As shown in Fig. 7(b), the mechanisms of the barrier leakage current include TE, Fowler–Nordheim (FN) tunneling, PF emission, and other trap-assisted emission. FN tunneling current can be can be given by [21]

$$J_{FN} = AE^2 \exp\left[-\frac{B}{E}\right] \tag{2}$$

with

$$B = \frac{8\pi\sqrt{2m_n^*(q\phi_{\rm eff})^3}}{3qh}$$

where A is a constant, m_n^* is the conduction-band effective mass in semiconductor, h is the Planck's constant, and $\phi_{\rm eff}$ is the effective barrier height. The FN tunneling process is independent on temperature, but strongly depends on electric field [23]. For conventional AlGaN/GaN HEMTs, TE and PF emission are two dominant mechanisms for reverse gate current [21]. Because of the large electric field resulting from the high spontaneous polarization charge, FN tunneling current becomes one of the dominant leakage currents in InAlN/GaN HEMTs [21]. PF emission and other trap-assisted emission can be depressed by improving the material quality.

Holes would concentrate at the AlGaN/GaN interface for the reverse gate bias. The reverse leakage mechanisms, TE, FN tunneling, PF emission, and other trap-assisted emission may exist for holes. The estimated ratio of conduction-to-valence band discontinuity is 65:35 for AlGaN/GaN HEMTs [24]. Thus, the valence band offset is much smaller than the conduction band offset. For the Al mole fraction of 30%, the valence band offset $\Delta EV = 0.35(E_{g,\rm AlGaN} - E_{g,\rm GaN}) = 0.35(4.24 - 3.4) = 0.294\,\rm eV$, which is a small barrier height for the holes. Therefore, the probabilities of the holes emission from the interface to the gate electrode by using the reverse leakage mechanisms are very high. The hole mobility is very low compared with electron mobility, and the hole leakage currents are rarely considered in previous studies. However, the hole leakage current should not be neglected when the number of the holes is very large.

For the mechanisms of the gate leakage current, hopping conduction and PF emission along the AlGaN surface, TE, PF emission, and other trap-assisted emission through the AlGaN barrier all increase with the increase of temperature. FN tunneling through the AlGaN barrier is independent on temperature. Therefore, the gate leakage current would increase at high temperature, and can exhibit a negative temperature coefficient.

The GaN buffer layer is not insulating, and a background doping (by Si or O impurities) exists in the GaN buffer layer. With the drain biased at a positive value, the buffer leakage current would be formed. With a higher temperature, the conduction of electrons through the buffer can be limited by the increased phonon scattering, which results in the reduction of the electron mobility and the buffer leakage current [25]. Therefore, the buffer leakage current has a positive temperature coefficient. However, electrons can be emitted from the trap energy levels to conduction band by the high temperature, increasing the electron density. It was observed that the buffer leakage experiences a large reduction from 20 °C to 70 °C, followed by a slow reduction above 70 °C [25]. The slow reduction is possibly due to the ionization of the shallow traps in the buffer layer. As a result, the buffer leakage current may exhibits a negative temperature coefficient in some cases.

For GaN-based HEMT, there exist two main breakdown mechanisms as follows:

1) The breakdown electric field strength for GaN material is 3.3 MV/cm, and the breakdown strength for AlGaN would be higher. If the electric field in the material cannot exceed the breakdown strength, it is thermal runaway that can cause the device breakdown. With the increase of $V_{\rm DS}$, the gate leakage and buffer leakage currents would increase to certain values. The leakage currents produce thermal energy, leading to the increase in temperature. The increased temperature would further increase the gate leakage current. It is a kind of uncontrolled positive feedback, leading to thermal runaway. If the buffer leakage current has a negative temperature coefficient, thermal runaway may be induced by the buffer leakage current. $V_{\rm BR}$ induced by thermal runaway has a negative temperature coefficient [20].
2) With a high $V_{\rm DS}$, a high electric field always locates at the drain-side edge of the gate terminal [26]. If the electric field peak exceeds the breakdown strength of the GaN-based materials, impact ionization would occur by the injection of electrons and holes, and then it can result in avalanche breakdown. $V_{\rm BR}$ induced by impact ionization exhibits a positive temperature coefficient [27]. The value of the injection current $I_{\rm inject}$ has an impact on the breakdown voltage $V_{\rm BR}$. The relation between $I_{\rm inject}$ and $V_{\rm BR}$ is given by [28]

$$I_{\rm inject} = \frac{E_i \Delta I_D}{qV_{\rm BR}} \exp\left[3E_p E_i \left(\frac{l}{q\lambda V_{\rm BR}}\right)^2\right] \tag{3}$$

where E_i is the threshold energy for electron–hole pair generation, ΔI_D is the increase in the drain current due to injection current $I_{\rm inject}$ and it is a constant value, E_p is the effective energy of the phonons involved in the scattering process, l is the length of the maximum-field region, and λ is the phonon scattering mean free path. It can be found that $V_{\rm BR}$ would decrease with the increase of the injection current. For GaN-based HEMTs, the injection current is the gate leakage or buffer leakage current.

For GaN-based HEMTs, thermal runaway and impact ionization can result in the device breakdown. Buffer leakage current induces the breakdown types A, C, and D, while the gate leakage current induces the breakdown types B, E, F, and G. Besides using techniques such as field plate to reduce the electric field peak [26], reducing the leakage current can alleviate both the thermal runaway and impact ionization process. Breakdown voltage enhancement of reducing the leakage current has been proved by numerous studies [16], [29]. Thus, the values of the leakage currents are very important for the investigation on breakdown mechanisms. Generally, the conventional 3-D breakdown characterization method is utilized to demonstrate these leakage currents and investigate breakdown mechanisms. It can be found that the conventional breakdown characterization method is not suitable to breakdown types C–G. The reasons are as follows:

1) The buffer leakage $I_{\rm ds}$ can be reduced by the adoption of AlGaN back barrier layer or carbon-doped GaN back barrier layer [16], [30]. In order to investigate the $V_{\rm BR}$ enhancement of the back barrier layer, it is very important to obtain the buffer leakage current values before and after the adoption of the back barrier layer. The source leakage current I_S is not the buffer leakage current $I_{\rm ds}$ due to the source-gate leakage current $I_{\rm sg}$. I_S deviates from $I_{\rm ds}$ severely in types C–G. Therefore, the conventional breakdown characterization method is not suitable to breakdown types C–G from the perspective of the buffer leakage current.
2) It is the drain-gate leakage current $I_{\rm dg}$, not the whole gate leakage current I_G, that flows from drain to gate, resulting in the gate-induced breakdown. I_G is not equal to $I_{\rm dg}$ due to the source-gate leakage current $I_{\rm sg}$. Although I_G can be used to investigate the gate-induced breakdown mechanisms in some cases, it is a rough analysis. It is more reasonable to compare $I_{\rm dg}$ values to investigate $V_{\rm BR}$ enhancement techniques. In order to investigate the breakdown mechanisms of types C–G precisely, the conventional breakdown characterization method should be modified.

After obtaining the $I_{\rm dg}$ value, the ratio of $I_{\rm dg,surface}$ and $I_{\rm dg,barrier}$ can be evaluated from the double gate structure [22]. The barrier leakage current values induced by TE, FN tunneling, PF emission, and other trap-assisted emission can be discriminated by temperature-dependent experiments to find out the dominant barrier leakage component [21]. Corresponding leakage-reduction techniques can be carried out after the determination of the dominant leakage component, and $V_{\rm BR}$ would be improved more effectively.

C. Time-Dependent Breakdown

Reliability is a very important issue for devices in practical applications. The breakdown could be happened when the GaN-based HEMTs are submitted to constant voltage stress, in the off-state [14], [31]–[33]. Fig. 5(h) and (i) exhibit two breakdown types for time-dependent breakdown. The stress conditions are $V_{\rm GS} < V_{\rm th}$ and $V_{\rm DS} = 0 \sim V_{\rm BR}$ (this $V_{\rm BR}$ is the breakdown voltage in the conventional breakdown curves). The stress condition of the Fig. 5(h) is the point $\rm A_1$ in type A as shown in Fig. 5(a). The stress condition of the Fig. 5(i) is the point $\rm B_1$ in type D as shown in Fig. 5(d). For types A and H, $|I_{\rm sg}|$ is smaller than $|I_{\rm ds}|$. Therefore, I_G and I_S and represent the gate leakage and buffer leakage currents, respectively. In contrast, $|I_{\rm sg}|$ in the type I cannot be neglected. I_S is the vector sum of $I_{\rm ds}$ and $I_{\rm sg}$, which flow in opposite direction. During the whole stress experiments, $I_{\rm sg}$ is a constant value due to the small electric field caused by $V_{\rm GS}$. The large $V_{\rm DS}$ forms a strong electric field in the buffer layer, and $I_{\rm ds}$ would increase with the increase of time due to the thermal positive feedback or impact ionization. When $|I_{\rm ds}|$ begins to exceed $|I_{\rm sg}|$, a inflection point on I_S curve emerges. $|I_S|$ would firstly decrease (before this inflection point), and then increase (after the inflection point). When the drain leakage current reaches 1 mA/mm, device breakdown would happen and the corresponding stress time is called as breakdown time $t_{\rm BR}$. Type I is not the only case for the point $\rm B_1$ in type D. If $|I_{\rm ds}|$ cannot exceed $|I_{\rm sg}|$ for the whole stress experiments, type I would change to another type. In addition, any point in types A $\sim$ G can be utilized to do time-dependent experiments. Therefore, there are many kinds of time-dependent breakdown types. However, these breakdown types can be explained using similar analysis as above. The time-dependent breakdown types as type I have the similar problem as types C $\sim$ G, and it is not reasonable to use conventional breakdown characterization method on such time-dependent breakdown types.

There are two cases for the stress conditions of the time-dependent breakdown.

1) $V_{\rm GS} < V_{\rm th}$ and $V_{\rm DS} = 0$ V. In this case, $I_{\rm ds} = 0$, $I_D = I_{\rm dg}$, and $I_{\rm S} = I_{\rm sg}$. Long stress times can result in the generation of a conductive (defective) path between gate and the buffer [31]. The gate leakage would increase suddenly due to the generation of parasitic leakage paths, leading to a permanent degradation and gate-induced breakdown. The stress time of the gate degradation showed strong gate bias dependence. For a larger reverse gate bias, the breakdown time $t_{\rm BR}$ would be shorter [32]. The weak temperature dependence of the gate leakage indicates that the gate degradation is a tunneling mechanism. The conventional breakdown characterization method is suitable to this case. Under this condition, it is more reasonable to utilize $I_G = 1$ mA/mm as the breakdown criterion instead of $I_D = 1$ mA/mm.
2) $V_{\rm GS} < V_{\rm th}$ and 0 V $< V_{\rm DS} < V_{\rm BR}$ (the breakdown voltage in the conventional breakdown curves) [14], [33]. In this case, thermal runaway and impact ionization can result in the device breakdown. Thus, it is necessary to use $I_{\rm ds}$ and $I_{\rm dg}$, rather than I_S and I_G, to characterize the breakdown mechanisms. In type I, I_S deviates from $I_{\rm ds}$ severely, indicating that the conventional breakdown characterization method is not suitable to type I. For a larger $V_{\rm DS}$, $t_{\rm BR}$ would be shorter. There exist two reasons for this dependence. First, $I_{\rm ds}$ and $I_{\rm dg}$ would be larger with the larger drain bias, which can produce more thermal energy and accelerate the thermal runaway process. Second, if impact ionization can occur at such a drain bias, a larger drain

bias would increase the impact ionization coefficient and accelerate impact ionization process.

For GaN-based HEMTs, the gate bias has an effect on the gate and buffer leakage currents [25], [34]. For a larger $|V_{\rm GS}|(V_{\rm GS} < V_{\rm th})$, the gate leakage current would increase due to a stronger electric field, while the buffer leakage current would decrease because of a deeper depletion region in the buffer layer. It is also unreasonable to compare I_S values to investigate the effect of the gate bias on buffer leakage for types C–G and I.

All the off-state leakage currents and possible breakdown curves have been investigated in this section. The conventional breakdown characterization method does not apply to conventional breakdown types C–G and time-dependent breakdown type I. The source-gate leakage current $I_{\rm sg}$ is the main reason for the difference between source leakage current I_S and buffer leakage current $I_{\rm ds}$. It is necessary to obtain the buffer leakage current to modify the conventional breakdown characterization method. In Section IV, we will extract the buffer leakage current by taking the devices demonstrated in this paper as examples.

IV. Modified Breakdown Characterization Method

There are six main leakage currents in GaN-based HEMTs as shown in Fig. 4. Although I_S, I_G, and I_D are known quantities, the vector sum of them is zero. Any one of them can be expressed by the other two quantities and there are actually two known quantities. As a result, the three unknown quantities, $I_{\rm sg}$, $I_{\rm dg}$, and $I_{\rm ds}$, cannot be solved by the known quantities I_S, I_G, and I_D directly.

$V_{\rm GS}$ remains constant during the breakdown measurements, hence $I_{\rm sg}$ can be assumed to be a constant value. In order to obtain the $I_{\rm sg}$ value, both the source and drain terminals should be biased at 0 V and the gate terminal should be set to the voltage which was used to test the breakdown voltage. Under this condition, $I_{\rm ds}$ is zero and the absolute value of I_S equals $I_{\rm sg}$. For the devices in this paper, $I_{\rm sg}$, $I_{\rm dg}$, and $I_{\rm ds}$ can be obtained by the following equations:

$$I_{\rm sg} = I_S|_{(V_{\rm GS}=-5{\rm V}, V_S=V_{\rm DS}=0{\rm V})} \quad (4)$$

$$I_{\rm ds} = -(I_S - I_{\rm sg}) \quad (5)$$

$$I_{\rm dg} = -I_G - I_{\rm sg} = I_D - I_{\rm ds}. \quad (6)$$

According to (4) and breakdown curves shown in Fig. 3, $I_{\rm sg}$ is 2.95×10^{-3} mA/mm for the SH HEMT and 1.23×10^{-3} mA/mm for the DH HEMT, respectively. $I_{\rm ds}$ and $I_{\rm dg}$ can be solved by using (5) and (6). As shown in Fig. 8, the buffer leakage current $I_{\rm ds}$ was reduced from $0.8 \sim 1.1 \times 10^{-3}$ mA/mm for the SH HEMT to $1.5 \sim 3.1 \times 10^{-4}$ mA/mm for the DH HEMT by using the AlGaN buffer layer. $I_{\rm dg}$ forms a part of I_D, and the value of it is smaller than that of I_D. I_G is the total leakage current on the gate terminal and it is also a very important off-state leakage current during the breakdown measurements. The purpose of solving $I_{\rm dg}$ is to explain the phenomenon that I_G exceeds I_D and present the leakage current flowing from the drain terminal to gate terminal, which may be necessary for the precise analysis of breakdown mechanisms. Because of the reduction of buffer leakage current, the buffer-induced breakdown for the SH HEMT was changed to the gate-induced breakdown for the DH HEMT. It can be observed that $I_{\rm ds}$ and $I_{\rm dg}$ are more reasonable to express the breakdown mechanisms compared with I_S and I_G. The modified breakdown characterization method is more suitable for the devices compared with the conventional breakdown characterization method.

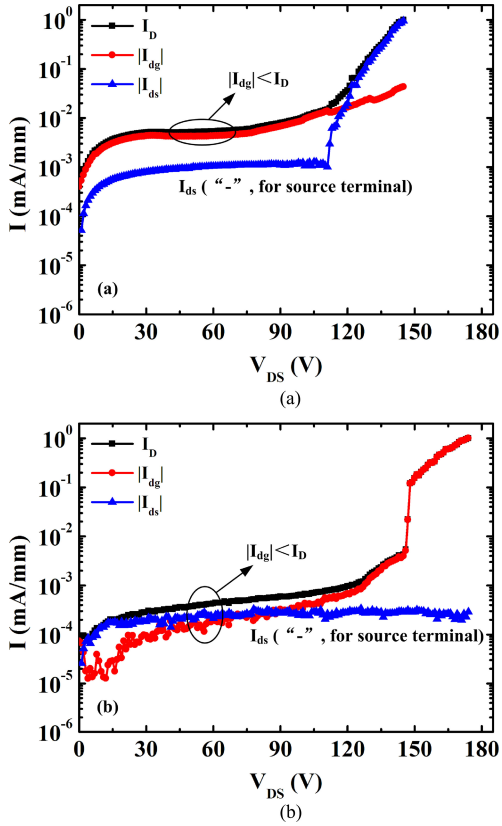

Fig. 8. $I_{\rm ds}$ and $I_{\rm dg}$ extracted from breakdown curves of the AlGaN/GaN (a) SH HEMT and (b) DH HEMT with VGS $= -5$ V.

The breakdown curves of AlGaN/GaN SH HEMT and DH HEMT can be categorized as types D and G, respectively. The modified breakdown characterization method also applies to other breakdown types. It is very essential to adopt the modified method to explore the breakdown mechanisms of GaN-based HEMTs with breakdown types C–G. For time-dependent breakdown type I, $I_{\rm sg}$ value can be extracted from the conventional breakdown curves (type D), and then $I_{\rm ds}$ and $I_{\rm dg}$ would be obtained from (5) and (6). The breakdown investigated in this paper is based on insulating substrate. The leakage currents and breakdown curves would be more complicated for conductive substrate, such as silicon substrate. Except the leakage currents discussed in this paper, other leakage currents would form if only the substrate terminal and metal terminals biased at different voltage values.

Besides the thermal runaway and impact ionization, the accumulation of positive charge in proximity of the gate can result in the device breakdown [14], [35], [36]. With gate biased at a negative value, holes would concentrate at the AlGaN/GaN interface as shown in Fig. 7(b). Holes may originate from defects in the GaN-based materials. For MIS structure, defects at the

dielectric/semiconductor interface may contribute to the generation of holes [35]. For a large drain bias, holes can be generated by the impact ionization process due to a high electric field particularly at the drain-side of the gate edge [36]. The generated holes would form gate leakage current by TE, FN tunneling, PF emission, and other trap-assisted emission. When the hole density is sufficient large, the hole leakage current cannot be neglected, even resulting in the gate-induced breakdown. The threshold voltage $V_{\rm th}$ would shift negatively due to the accumulation of the holes at the AlGaN/GaN interface. The negative shift of $V_{\rm th}$ changes the off state of the device to semi-on state, resulting in an increase of the buffer leakage current [14]. In stress experiments, a sudden increase of the buffer leakage current, corresponding to permanent degradation, can be detected for a sufficient long stress time. This catastrophic failure possibly is due to thermal runaway or impact ionization in proximity of the localized drain-source leakage paths. The holes may be generated in proximity of the drain-side of the gate, and immediately move to the source-side of the gate [35], which may increase the source-gate leakage current $I_{\rm sg}$. Therefore, $I_{\rm sg}$ may not be a constant value after the accumulation of holes. For hole-induced breakdown types, the leakage currents extracted from the modified breakdown characterization method may be not entirely correct. However, $I_{\rm sg}$ is a constant value before the accumulation of holes, and the modified method is still helpful to investigate the leakage currents and breakdown mechanisms.

V. Conclusion

The breakdown characterization method in GaN-based HEMTs has been analyzed in this paper. The conventional breakdown characterization method does not apply to conventional breakdown types C–G and time-dependent breakdown type I. Discussions of the off-state leakage currents and breakdown curves indicate that the conventional breakdown characterization method should be modified to explore the breakdown mechanisms correctly. The buffer leakage current was extracted by assuming the source-gate leakage current as a constant value. A modified breakdown characterization method was proposed based on this extraction method. The reduction of the buffer leakage current in the DH HEMTs has been verified by the modified breakdown characterization method. Experiments indicate that the modified breakdown characterization method is worth popularizing for investigating the breakdown mechanisms in GaN-based HEMTs.

In order to illustrate the relation between breakdown curves and breakdown mechanisms, the relation between leakage currents and breakdown mechanisms has been analyzed carefully. Leakage current mechanisms, including hopping conduction and PF emission along the AlGaN surface, TE, FN tunneling, PF emission, and other trap-assisted emission through the AlGaN barrier, and the buffer leakage, have been presented and analyzed. The relation between leakage currents and two important breakdown mechanisms, thermal runaway and impact ionization, has been discussed. It is found that leakage current values can affect thermal runaway and impact ionization. Reducing the leakage current can alleviate both the thermal runaway and impact ionization process, improving breakdown voltage. Therefore, the values of the leakage currents are very important to investigate breakdown mechanisms. $I_{\rm ds}$ and $I_{\rm dg}$ are the leakage currents inducing thermal runaway and impact ionization. In some cases (types C–G and I), I_S and I_G cannot represent these two leakage currents. Therefore, the conventional breakdown characterization method should be modified to explore the breakdown mechanisms correctly. Besides the thermal runaway and impact ionization, the accumulation of positive charge in proximity of the gate can result in the device breakdown. The modified characterization method is also helpful to the investigation on the leakage currents and breakdown mechanisms for the case of the accumulation of positive charge.

References

[1] T. Imada, M. Kanamura, and T. Kikkawa, "Enhancement-mode GaN MIS-HEMTs for power supplies," in *Proc. IEEE Power Electron. Conf.*, 2010, pp. 1027–1033.

[2] J. L. Hudgins, G. S. Simin, E. Santi, and M. A. Khan, "An assessment of wide bandgap semiconductors for power devices," *IEEE Trans. Power Electron.*, vol. 18, no. 3, pp. 907–914, May 2003.

[3] U. K. Mishra, P. Parikh, and Y.-F. Wu, "AlGaN/GaN HEMTs-an overview of device operation and applications," *Proc. IEEE*, vol. 90, no. 6, pp. 1022–1031, Jun. 2002.

[4] H. Xing, Y. Dora, A. Chini, S. Heikman, S. Keller, and U. K. Mishra, "High breakdown voltage AlGaN–GaN HEMTs achieved by multiple field plates," *IEEE Electron Device Lett.*, vol. 25, no. 4, pp. 161–163, Apr. 2004.

[5] Y.-F. Wu, J. Gritters, L. Shen, R. P. Smith, and B. Swenson, "kV-class GaN-on-Si HEMTs enabling 99% efficiency converter at 800 V and 100 kHz," *IEEE Trans. Power Electron.*, vol. 29, no. 6, pp. 2634–2637, Jun. 2014.

[6] M. Rodríguez, Y. Zhang, and D. Maksimović, "High-frequency PWM buck converters using GaN-on-SiC HEMTs," *IEEE Trans. Power Electron.*, vol. 29, no. 5, pp. 2462–2473, May 2014.

[7] K. Zhang, M. Y. Cao, Y. H. Chen, L. Y. Yang, C. Wang, X. H. Ma, and Y. Hao, "Fabrication and characterization of V-gate AlGaN/GaN high-electron-mobility transistors," *Chin. Phys. B*, vol. 22, no. 5, pp. 057304-1–057304-4, 2013.

[8] S. L. Zhao, J. S. Xue, P. Zhang, B. Hou, J. Luo, X. J. Fan, J. C. Zhang, X. H. Ma, and Y. Hao, "Enhancement-mode Al_2O_3/InAlN/AlN/GaN metal–insulator–semiconductor high-electron-mobility transistor with enhanced breakdown voltage using fluoride-based plasma treatment," *Appl. Phys. Exp.*, vol. 7, no. 7, pp. 071002-1–071002-4, Jul. 2014.

[9] Q. Zhou, H. Chen, C. Zhou, Z. H. Feng, S. J. Cai, and K. J. Chen, "Schottky source/drain InAlN/AlN/GaN MISHEMT with enhanced breakdown voltage," *IEEE Electron Device Lett.*, vol. 33, no. 1, pp. 38–40, Jan. 2012.

[10] H. S. Lee, D. Piedra, M. Sun, X. Gao, S. Guo, and T. Palacios, "3000-V 4.3-m$\Omega\cdot$cm^2 InAlN/GaN MOSHEMTs with AlGaN back barrier," *IEEE Electron Device Lett.*, vol. 33, no. 7, pp. 982–984, Jul. 2012.

[11] L. Yuan, H. Chen, and K. J. Chen, "Normally off AlGaN/GaN metal–2DEG tunnel-junction field-effect transistors," *IEEE Electron Device Lett.*, vol. 32, no. 3, pp. 303–305, Mar. 2011.

[12] T. Nanjo, A. Imai, Y. Suzuki, Y. Abe, T. Oishi, M. Suita, E. Yagyu, and Y. Tokuda, "AlGaN channel HEMT with extremely high breakdown voltage," *IEEE Trans. Electron Devices*, vol. 60, no. 3, pp. 1046–1053, Mar. 2013.

[13] Y. Liu, S. P. Singh, Y. J. Ngoo, L. M. Kyaw, M. K. Bera, Q. Q. Lo, and E. F. Chor, "Low thermal budget Hf/Al/Ta ohmic contacts for InAlN/GaN-on-Si HEMTs with enhanced breakdown voltage," *J. Vac. Sci. Technol. B*, vol. 32, no. 3, pp. 032201-1–032201-7, 2014.

[14] M. Meneghini, G. Cibin, M. Bertin, G. A. M. Hurkx, P. Ivo, J. Šonský, J. A. Croon, G. Meneghesso, and E. Zanoni, "OFF-state degradation of AlGaN/GaN power HEMTs: Experimental demonstration of time-dependent drain-source breakdown," *IEEE Trans. Electron Devices*, vol. 61, no. 6, pp. 1987–1992, Jun. 2014.

[15] Q. Zhou, W. Chen, S. Liu, B. Zhang, Z. Feng, S. Cai, and K. J. Chen, "Schottky-contact technology in InAlN/GaN HEMTs for breakdown voltage improvement," *IEEE Trans. Electron Devices*, vol. 60, no. 3, pp. 1075–1081, Mar. 2013.

[16] E. Bahat-Treidel, O. Hilt, F. Brunner, J. Würfl, and G. Tränkle, "Punchthrough-voltage enhancement of AlGaN/GaN HEMTs using

AlGaN double-heterojunction confinement," *IEEE Trans. Electron Devices*, vol. 55, no. 12, pp. 3354–3359, Dec. 2008.
[17] J. Ma, J. Zhang, J. Xue, Z. Lin, Z. Liu, X. Xue, X. Ma, and Y. Hao, "Characteristics of AlGaN/GaN/AlGaN double heterojunction HEMTs with an improved breakdown voltage," *J. Semicond.*, vol. 33, no. 1, pp. 014002-1–014002-5, Jan. 2012.
[18] R. J. Trew, D. S. Green, and J. B. Shealy, "AlGaN/GaN HFET reliability," *IEEE Microw. Mag.*, vol. 10, no. 4, pp. 116–127, Jun. 2009.
[19] Y. H. Chen, K. Zhang, M. Y. Cao, S. L. Zhao, J. C. Zhang, X. H. Ma, and Y. Hao, "Study of surface leakage current of AlGaN/GaN high electron mobility transistors," *Appl. Phys. Lett.*, vol. 104, no. 15, pp. 153509-1–153509-4, Apr. 2014.
[20] W. S. Tan, P. A. Houston, P. J. Parbrook, D. A. Wood, G. Hill, and C. R. Whitehouse, "Gate leakage effects and breakdown voltage in metalorganic vapor phase epitaxy AlGaN/GaN heterostructure field-effect transistors," *Appl. Phys. Lett.*, vol. 80, no. 17, pp. 3207–3209, Apr. 2002.
[21] S. Turuvekere, N. Karumuri, A. A. Rahman, A. Bhattacharya, A. DasGupta, and N. DasGupta, "Gate leakage mechanisms in AlGaN/GaN and AlInN/GaN HEMTs: Comparison and modeling," *IEEE Trans. Electron Devices*, vol. 60, no. 10, pp. 3157–3165, Oct. 2013.
[22] W. S. Tan, M. J. Uren, P. A. Houston, R. T. Green, R. S. Balmer, and T. Martin, "Surface leakage currents in SiN_x passivated AlGaN/GaN HFETs," *IEEE Electron Device Lett.*, vol. 27, no. 1, pp. 1–3, Jan. 2006.
[23] L. Xia, A. Hanson, T. Boles, and D. Jin, "On reverse gate leakage current of GaN high electron mobility transistors on silicon substrate," *Appl. Phys. Lett.*, vol. 102, no. 11, pp. 113510-1–113510-4, Mar. 2013.
[24] D. R. Hang, C. H. Chen, Y. F. Chen, H. X. Jiang, and J. Y. Lin, "$Al_xGa_{1-x}N$/GaN band offsets determined by deep-level emission," *J. Appl. Phys.*, vol. 90, no. 4, pp. 1887–1890, Aug. 2001.
[25] M. Wang and K. J. Chen, "Off-state breakdown characterization in AlGaN/GaN HEMT using drain injection technique," *IEEE Trans. Electron Devices*, vol. 57, no. 7, pp. 1492–1496, Jul. 2010.
[26] S. Karmalkar and U. K. Mishra, "Enhancement of breakdown voltage in AlGaN/GaN high electron mobility transistors using a field plate," *IEEE Trans. Electron Devices*, vol. 48, no. 8, pp. 1515–1512, Aug. 2001.
[27] N. Dyakonova, A. Dickens, M. S. Shur, R. Gaska, and J. W. Yang, "Temperature dependence of impact ionization in AlGaN-GaN heterostructures field effect transistors," *Appl. Phys. Lett.*, vol. 72, no. 20, pp. 2562–2564, May 1998.
[28] T. Nakao, Y. Ohno, S. Kishimoto, K. Maezawa, and T. Mizutani, "Study on off-state breakdown in AlGaN/GaN HEMTs," *Phys. Stat. Sol. (C)*, vol. 0, no. 7, pp. 2335–2338, Dec. 2003.
[29] H. S. Lee, D. Piedra, M. Sun, X. Gao, S. Guo, and T. Palacios, "3000-V 4.3-m$\Omega\cdot$cm^2 InAlN/GaN MOSHEMTs with AlGaN back barrier," *IEEE Electron Device Lett.*, vol. 33, no. 7, pp. 982–984, Jul. 2012.
[30] E. Bahat-Treidel, F. Brunner, O. Hilt, E. Cho, J. Würfl, and G. Tränkle, "AlGaN/GaN/GaN:C back-barrier HFETs with breakdown voltage of over 1 kV and low $R_{ON}\times A$," *IEEE Trans. Electron Devices*, vol. 57, no. 11, pp. 3050–3058, Nov. 2010.
[31] M. Meneghini, A. Stocco, M. Bertin, D. Marcon, A. Chini, G. Meneghesso, and E. Zanoni, "Time-dependent degradation of AlGaN/GaN high electron mobility transistors under reverse bias," *Appl. Phys. Lett.*, vol. 100, pp. 033505-1–033505-3, 2012.
[32] D. Marcon, G. Meneghesso, T. L. Wu, S. Stoffels, M. Meneghini, E. Zanoni, and S. Decoutere, "Reliability analysis of permanent degradations on AlGaN/GaN HEMTs," *IEEE Trans. Electron Devices*, vol. 60, no. 10, pp. 3132–3141, Oct. 2013.
[33] M. Meneghini, D. Bisi, D. Marcon, S. Stoffels, M. V. Hove, T. L. Wu, S. Decoutere, G. Meneghesso, and E. Zanoni, "Trapping and reliability assessment in D-Mode GaN-based MIS-HEMTs for power applications," *IEEE Trans. Power Electron.*, vol. 29, no. 5, pp. 2199–2207, May 2014.
[34] M. Meneghini, A. Zanandrea, F. Rampazzo, A. Stocco, M. Bertin, G. Cibin, D. Pogany, E. Zanoni, and G. Meneghesso, "Electrical and electroluminescence characteristics of AlGaN/GaN high electron mobility transistors operated in sustainable breakdown conditions," *Jpn. J. Appl. Phys.*, vol. 52, no. 8, pp. 08JN17-1–08JN17-4, 2013.
[35] S. R. Bahl, M. V. Hove, X. Kang, D. Marcon, M. Zahid, and S. Decoutere, "New source-side breakdown mechanism in AlGaN/GaN insulated-gate HEMTs," in *Proc. 25th Int. Symp. Power Semicond. Devices ICs*, May 2013, pp. 419–422.
[36] H. Hanawa, H. Onodera, A. Nakajima, and K. Horio, "Numerical analysis of breakdown voltage enhancement in AlGaN/GaN HEMTs with a high-*k* passivation layer," *IEEE Trans. Electron Devices*, vol. 61, no. 3, pp. 769–775, Mar. 2014.

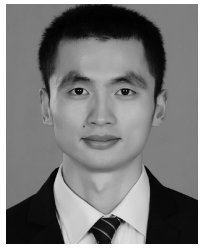

Sheng Lei Zhao received the B.S. degree from Xidian University, Xi'an, China, in 2010. He is currently working toward the Ph.D. degree at the School of Microelectronics, Xidian University.

His research interests include GaN-based and Si-based power electronics.

Bin Hou received the B.S. degree from Xidian University, Xi'an, China, in 2011. He is currently working toward the Ph.D. degree at the School of Advanced Materials and Nanotechnology, Xidian University.

His research interests include GaN-based enhancement-mode and microwave devices.

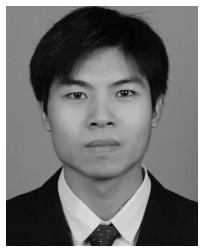

Wei Wei Chen received the B.S. degree from Xidian University, Xi'an, China, in 2011. He is currently working toward the Ph.D. degree at the School of Advanced Materials and Nanotechnology, Xidian University.

His research interests include fabrication, characterization and reliability analysis of GaN-based high-electron-mobility transistors.

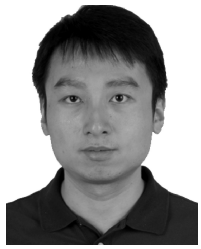

Min Han Mi received the B.S. degree from Xidian University, Xi'an, China, in 2011. He is currently working toward the Ph.D. degree at the School of Microelectronics, Xidian University.

His research interests include GaN-based microwave and millimeterwave devices.

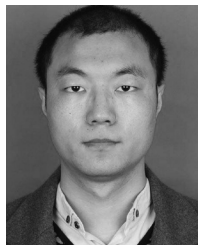

Jia Xin Zheng received the B.S. degree from Xidian University, Xi'an, China, in 2013. He is currently working toward the Ph.D. degree at the School of Advanced Materials and Nanotechnology, Xidian University.

His research interests include GaN-based microwave and millimeterwave circuit design.

Jin Cheng Zhang received the Ph.D. degree from Xidian University, Xi'an, China, in 2004.

He is currently a Professor at the School of Microelectronics, Xidian University. His research interests include the material growth and characterization of GaN-based heterojunctions.

Xiao Hua Ma (M'08) received the Ph.D. degree from Xidian University, Xi'an, China, in 2007.

He is currently a Professor at the School of Advanced Materials and Nanotechnology, Xidian University. His research interests include GaN-based microwave and millimeterwave devices, enhancement-mode devices and power electronics devices.

Yue Hao (SM'92) received the Ph.D. degree from Xi'an Jiaotong University, Xi'an, China, in 1990.

He is currently a Professor at the School of Microelectronics, Xidian University, Xi'an. His research interests include GaN-based and SiC-based materials and devices, nanodevices and technology, semiconductor device reliability physics and failure mechanism, terahertz semiconductor materials and devices, and organic electronics.